


Ultrafast and anharmonic Rabi oscillations between non-Bloch bands

Ching Hua Lee ¹✉ & Stefano Longhi^{2,3}✉

Bloch band theory and bulk-boundary correspondence in non-Hermitian systems are attracting great attention in different areas of science. Interband transitions and Rabi flopping induced by emission or absorption of field quanta are fundamental and well-understood processes in Hermitian systems. However, they are challenged in a non-Hermitian system, where band theory is affected by system boundaries. Here we consider Rabi oscillations in non-Hermitian lattices exhibiting unbalanced non-Hermitian skin effect, and unveil an unprecedented scenario of Rabi flopping. The effective dipole moment of the transition - usually considered a bulk property - is however strongly dependent on boundary conditions. Rabi oscillations become anharmonic and transitions cease to be vertical in the energy-momentum plane in systems with open boundaries. Remaining stable even in the presence of complex energies, Rabi oscillations provide a vivid illustration of how competition between non-Hermitian, non-local and Floquet effects can result in significant enhancements of physically measurable quantities.

¹ Department of Physics, National University of Singapore, Singapore 117542, Singapore. ² Dipartimento di Fisica, Politecnico di Milano and Istituto di Fotonica e Nanotecnologie del Consiglio Nazionale delle Ricerche, Piazza L. da Vinci 32, Milano 20133, Italy. ³ IFISC (UIB-CSIC), Instituto de Física Interdisciplinaria Sistemas Complejos, Palma de Mallorca E-07122, Spain. ✉email: phylch@nus.edu.sg; stefano.longhi@polimi.it

The coherent dynamics of electrons in crystalline potentials under time-periodic driving fields is at the heart of such major phenomena as photon-assisted transport, Rabi oscillations (ROs), dynamic localization, and super-Bloch oscillations^{1–18}. Strong ac fields can modify the band structures of materials and alter the corresponding internal structure of the electronic wave functions^{19–23}, whereas weak ac fields in resonance with two bands of the crystal can induce interband transitions, e.g., absorption and emission of quanta from the field. Momentum conservation ensures that direct transitions must be vertical in the (k, E) plane during absorption and emission, where k and E are the quasi-momentum and energy of the electron. Under coherent dynamics, periodic electron flopping, i.e., ROs between two Bloch bands, can be observed^{4,5,8}. The characteristic frequency of the Rabi flopping is proportional to the electric-dipole moment of the transition and the field strength. In condensed matter systems, dephasing effects generally prevent the observation of Rabi flopping. For such a reason, ROs have been observed mostly in synthetic lattices, such as in cold atoms and photonic crystals^{5,14}.

Topological properties, transport and phase transitions in non-Hermitian crystals, i.e., described by an effective non-Hermitian Hamiltonian, have attracted a huge interest in the past few years^{24–54}. In such crystals, the energy spectrum is strongly sensitive to perturbations, and largely differs under periodic (PBC) and open (OBC) boundary conditions. In systems with OBC the bulk states can get squeezed toward the lattice edges (non-Hermitian skin effect^{25–29,44,53}), and the bulk-boundary correspondence based on Bloch band topological invariants generally fails to predict topological edge states. To correctly describe energy spectra and topological invariants in crystals with OBC one needs to extend Bloch band theory so as the quasi-momentum becomes complex and varies on a generalized Brillouin zone (GBZ)^{25,26,28,34,44}. Bloch and non-Bloch bands show different energy spectra and can undergo different symmetry breaking phase transitions. As major attention is currently devoted to study the topological properties and related symmetries in several non-Hermitian models, the impact of the skin effect on bulk transport properties in non-Hermitian lattices driven by external fields remains so far largely unexplored.

In this work, we show how non-Hermitian influences can disclose a scenario fully distinct from common Rabi flopping, hosting novel features such as enhancement of the effective dipole

moment arising from the non-Hermitian skin effect, non-vertical transitions and anharmonic ROs, hence providing unprecedented freedom in controlling the frequency and anharmonicity of ROs. While non-Hermitian systems with complex eigenenergies have often been considered to be of limited experimental interest, since complex eigenenergies seem to lead to rapid decay or divergences, ROs can be sustained without gain or loss, even if the eigen-spectrum is complex. This thus greatly expands the scope by which ROs can be controlled or engineered, achieving Rabi frequencies that are orders of magnitudes higher than allowed by the bare dipole moments. More generally, our study sheds light on how non-Hermiticity further enriches the already vibrant field of Floquet dynamics^{55–57} beyond merely causing gain or attenuation.

Results

ROs in a non-Hermitian lattice. Let us consider a minimal non-Hermitian one-dimensional (1D) system comprising two identical chains (sublattices) H_O coupled by an inter-chain coupling term H_C . Acting on the system is a weak ac field $F(t) = F_0 \cos(\omega t)$ that staggers the energy of the two sublattices and drives the ROs. The system is thus described by a two-component Hamiltonian in real space

$$H(t) = \begin{pmatrix} H_O & H_C \\ H_C & H_O \end{pmatrix} - d_y F(t) \begin{pmatrix} \mathcal{I} & 0 \\ 0 & -\mathcal{I} \end{pmatrix}, \quad (1)$$

where $2d_y$ is the spatial separation between the two chains of length N , and \mathcal{I} is the $N \times N$ identity matrix (Fig. 1a). Diagonalizing $H(t)$ in the zero field limit via a basis transformation $H \rightarrow U^{-1} H U$ with $U = \frac{1}{\sqrt{2}} \begin{pmatrix} 1 & 1 \\ 1 & -1 \end{pmatrix}$, our system takes the form of two effective but inequivalent chains $H_{\pm} = H_O \pm H_C$ that are coupled by the oscillatory field $F(t)$ (Fig. 1b). In this new basis built from the symmetric and antisymmetric sectors, a two-component state $|\psi(t)\rangle = (|\mathbf{A}\rangle, |\mathbf{B}\rangle)^T$ obeys the dynamical evolution equation $i \frac{d\psi}{dt} = H\psi$ which reads

$$i \frac{d}{dt} \begin{pmatrix} \mathbf{A} \\ \mathbf{B} \end{pmatrix} = \left[\begin{pmatrix} H_+ & 0 \\ 0 & H_- \end{pmatrix} - d_y F(t) \begin{pmatrix} 0 & \mathcal{I} \\ \mathcal{I} & 0 \end{pmatrix} \right] \begin{pmatrix} \mathbf{A} \\ \mathbf{B} \end{pmatrix}. \quad (2)$$

To solve Eq. (2), we expand $|\mathbf{A}\rangle$ and $|\mathbf{B}\rangle$ in terms of the right eigenvectors $|u_{+,n}^R\rangle$ and $|u_{-,n}^R\rangle$, respectively, defined by

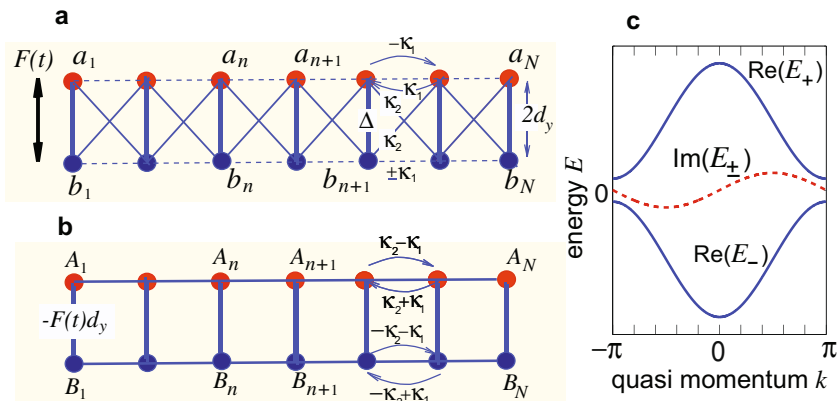


Fig. 1 Driven two-band lattices. **a** Schematic of an ac-driven non-Hermitian lattice formed by two chains with sites displayed by blue and red circles. The dashed thin black bonds denote a non-Hermitian hopping, with amplitudes $\pm \kappa_1$ depending on the direction (left/right) of the hopping, while solid black bonds describe Hermitian hopping. **b** Equivalent lattice after the basis transformation. The system is basically equivalent to two Hatano-Nelson chains, shifted in energy by $\pm \Delta$ and side-coupled by the oscillating bond $-d_y F(t)$. The skin modes under open boundary conditions are squeezed toward opposite edges in the two chains with the same skin length. **c** Energy bands under periodic boundary conditions in the undriven case ($F = 0$). Solid blue and dashed red lines refer to the real and imaginary parts of the energy spectrum, respectively.

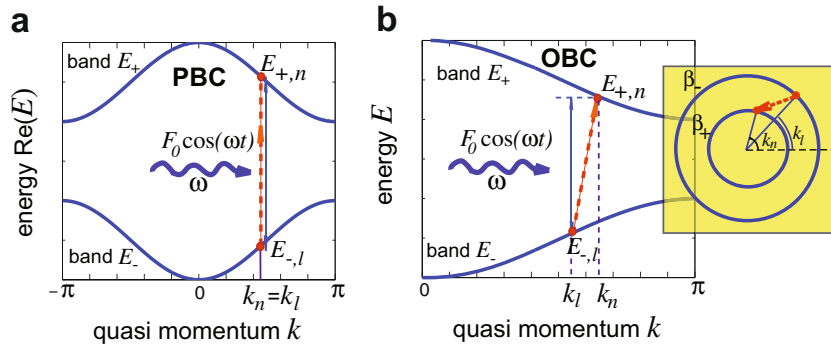


Fig. 2 Interband transitions and Rabi oscillations. **a** Field-induced transitions between Bloch bands in a system with periodic boundary conditions (PBC). The allowed transitions (vertical dashed lines) are vertical in the momentum–energy (k, E) plane. The resulting Rabi oscillations are always harmonic. **b** Under open boundary conditions (OBC), transitions between non-Bloch bands can be oblique in the (k, E) plane. Mixed transitions lead to anharmonic Rabi oscillations. The inset in **b** shows the two generalized Brillouin zones $\beta_{\pm} = \exp(\mp h + ik)$ and $\beta_{\pm} = \exp(h + ik)$ of upper and lower bands, corresponding to two circles (in blue color) of different radius $\exp(\mp h)$. Oblique transitions that do not conserve k correspond to non-radial jumps between the two generalized Brillouin zones, as shown by the dashed red arrow in the inset connecting the inner and outer circles.

$$H_{\pm} |u_{\pm,n}^R\rangle = E_{\pm,n} |u_{\pm,n}^R\rangle; \quad |\mathbf{A}\rangle = \sum_n \alpha_n(t) e^{-iE_{+,n}t} |u_{+,n}^R\rangle, \quad (3)$$

$$|\mathbf{B}\rangle = \sum_n \beta_n(t) e^{-iE_{-,n}t} |u_{-,n}^R\rangle. \quad (4)$$

Upon substituting into Eq. (2) and left multiplying by left eigenvectors defined by $H_{\pm}^{\dagger} |u_{\pm,n}^L\rangle = E_{\pm,n}^* |u_{\pm,n}^L\rangle$ and obeying the biorthogonal normalization $\langle u_{\pm,n}^L | u_{\pm,l}^R \rangle = \delta_{nl}$, we obtain coupled equations describing the evolution of the amplitude probabilities $\alpha_n(t)$ and $\beta_n(t)$ of the symmetric/antisymmetric sectors:

$$i \frac{d\alpha_n(t)}{dt} = -d_y F(t) \sum_l \Gamma_{n,l} \beta_l(t) e^{i(E_{+,n} - E_{-,l})t}, \quad (5)$$

$$i \frac{d\beta_l(t)}{dt} = -d_y F(t) \sum_n G_{l,n} \alpha_n(t) e^{i(E_{-,l} - E_{+,n})t}, \quad (6)$$

where $\Gamma_{n,l} = \langle u_{+,n}^L | u_{-,l}^R \rangle$ and $G_{l,n} = \langle u_{-,l}^L | u_{+,n}^R \rangle$. Without any restriction on the forms of $H_{\pm} = H_0 \pm H_C$, Eqs. (5) and (6) generically describe wildly fluctuating dynamics that is generically aperiodic with complex quasi-energy spectrum. To investigate ROs, we specialize to cases where well-defined oscillations exist between two chosen eigenstates $|u_{+,n}^R\rangle$ and $|u_{-,l}^R\rangle$ having the same growth/decay rate, i.e., vanishing imaginary part of $E_{+,n} - E_{-,l}$ (Fig. 1c), and make the crude rotating wave approximation (RWA), assuming as usual that $F(t)$ is modulated at resonance $\omega = \omega_{nl} \equiv E_{+,n} - E_{-,l}$ and the Rabi frequency is much smaller than ω . Neglecting all non-resonant and cross-coupling terms, from Eqs. (5) and (6) harmonic oscillator equations for the coupled amplitudes α_n and β_l are obtained, namely $\frac{d^2\alpha_n(t)}{dt^2} + \frac{1}{4}(d_y^2 F_0^2 \Gamma_{n,l} G_{l,n}) \alpha_n(t) = 0$ (and similarly for $\beta_l(t)$). The Rabi frequency is thus

$$\Omega_R = d_y F_0 \sqrt{|\Gamma_{n,l} G_{l,n}|} = d_y F_0 \sqrt{|\text{Tr}[P_n^+ P_l^-]|}, \quad (7)$$

where $P_{\mu}^{\pm} = |u_{\pm,\mu}^R\rangle \langle u_{\pm,\mu}^L|$ is the biorthogonal projector onto the μ th eigenstate of $H_{\pm} = H_0 \pm H_C$. (We have $\Gamma_{n,l} G_{l,n} = \langle u_{+,n}^L | u_{-,l}^R \rangle \langle u_{-,l}^L | u_{+,n}^R \rangle = \text{Tr}[P_n^+ P_l^- P_n^+] = \text{Tr}[P_n^+ P_l^-]$ since P_n^+ is idempotent.) Note that ROs can occur even in the absence of a real spectrum, as long as $E_{+,n} - E_{-,l}$ is real. Under PBCs, this reality condition simplifies to the requirement that H_C has a real spectrum. Equation (7) shows that the Rabi frequency Ω_R is

proportional to the effective dipole moment $\mu_{n,l}^{(\text{eff})} \equiv d_y \sqrt{|\text{Tr}[P_n^+ P_l^-]|}$, which can be enhanced in a non-Hermitian system. In the Hermitian case, this is not possible as $\text{Tr}[P_n^+ P_l^-] = |\langle u_{+,n} | u_{-,l} \rangle|^2 \leq 1$, with overlap integrals bounded above by unity. But in non-Hermitian cases, eigenstates are biorthogonally normalized, and there are two scenarios where $\text{Tr}[P_n^+ P_l^-]$ can be very large: (i) near an exceptional point and (ii) in the presence of boundary eigenmode accumulation, also known as the non-Hermitian skin effect. For (i), exceptional points have been known to harbor pronounced sensitivity due to the defective nature of their eigenspaces, and the dipole moment amplification is expected¹⁷. But more interesting is (ii), where the effective dipole moment and hence Rabi frequency can be controlled just by changing boundary conditions. Moreover, when considering ROs in the (k, E) plane, in the non-Hermitian case boundary conditions drastically challenge the common wisdom that transitions have to be vertical and harmonic, as discussed below.

Boundary-driven ultrafast and non-vertical ROs. The eigenvectors $|u_{\pm,n}^{R,L}\rangle$, and thus the scalar products $\Gamma_{n,b} G_{ml}$ defining the interband transitions, depend on the boundary conditions, and differ for PBC and OBC. Under PBC, $\langle x | u_{\pm,n}^{R,L} \rangle = \exp(iknx)$ are plane waves with quantized quasi-momentum $k_n = 2n\pi/N$, and thus $\Gamma_{n,b} G_{ml}$ vanish for $n \neq l$, i.e., the ac field can induce only vertical transitions in (k, E) plane, both for Hermitian and non-Hermitian systems (Fig. 2a). Correspondingly, ROs are always harmonic and there is not any enhancement of the dipole moment ($\mu_{n,n}^{(\text{eff})} = d_y$). Under OBC, the quasi-momentum k is not anymore a good quantum number^{58–61}; however, one can still diagonalize H_{\pm} in real space and the bulk energy spectrum (with the exception of isolated states) can be obtained from the GBZ^{25,28,34}, i.e., from the analytic continuation of the Bloch energy bands $E_{\pm}(k)$ where k becomes complex and spans, for each band, a path in complex plane, as detailed in the “Methods” (see also ref. 44). Here we focus our attention to the most interesting case where $H_{\pm}(k)$, under PBC, can be derived from the same momentum-space Hermitian Hamiltonian $H_H(k)$ via uniform complex momentum deformations $k \rightarrow k - ih_{\pm}$, i.e., $H_{\pm}(k) = Q_{\pm} H_H(k - ih_{\pm})$ with Q_{\pm} and h_{\pm} real parameters. This case applies to the typical scenario of ROs in lattices with nearest-neighbor (NN) hopping⁴, in which the non-Hermitian deformations h_{\pm} are introduced by synthetic imaginary gauge fields^{28,62–64}. As explained in the “Methods”, under OBC H_{\pm} show an entirely real

energy spectrum and share the same eigenmodes with quantized wave number $k_{+,n} = k_{-,n} \equiv k_n = \frac{n\pi}{N+1}$, $n = 1, 2, \dots, N$. In the Hermitian limit $h_1 = h_2 = 0$, one has $\Gamma_{nl} = G_{n,l} = 0$ for $l \neq n$ and ROs occur under resonance driving between eigenmodes in the two bands with the same quasi-momentum $k_n = k_l$ (Fig. 2a). In other words, ROs in the Hermitian limit are the same for PBC and OBC, and transitions remain vertical in the (k, E) plane. This is not the case for non-Hermitian lattices, where boundary conditions affect the dynamics tremendously as non-vertical transitions are allowed (Fig. 2b).

To illustrate this point, let us consider the NN Hamiltonian $H_H(k) = 2\sqrt{\kappa_2^2 - \kappa_1^2} \cos k + \Delta$, with Δ and $\kappa_2 > \kappa_1$ real and positive parameters, and let us assume $Q_{\pm} = \pm 1$ and $h_{\pm} = \mp h$ with $h = (1/2)\log[(\kappa_2 + \kappa_1)/(\kappa_2 - \kappa_1)]$. The resulting Hamiltonians H_{\pm} read

$$H_{\pm}(k) = 2i\kappa_1 \sin k \pm (\Delta + 2\kappa_2 \cos k) \quad (8)$$

corresponding to the physical single chain Hamiltonian $H_O = 2i\kappa_1 \sin k$ and inter-chain coupling $H_C = \Delta + 2\kappa_2 \cos k$; see Fig. 1a. After the basis transformation, the two decoupled lattices H_{\pm} are two Hatano–Nelson chains^{62–64} with asymmetric left/right hopping and shifted in energy by $\pm\Delta$; see Fig. 1b. The skin effect squeezes the bulk modes for the two bands towards opposite boundaries. To have well-spaced bands for ROs, we assume that the two bands are separated by a wide gap, i.e., we assume that $\Delta \gg \kappa_2$. Under PBCs, ROs occur only for vertical transitions $k_n = k_l$ [Fig. 2a], with corresponding eigenmodes displaying the same lifetime [Fig. 1c]. But under OBC the spectra of the two non-Bloch bands are entirely real and non-vertical transitions are allowed. The OBC energy spectra are readily obtained from the one of H_H and read

$$E_{\pm,n} = \pm \left[2\sqrt{\kappa_2^2 - \kappa_1^2} \cos k_n + \Delta \right] \quad (9)$$

with $k_n = n\pi/(N+1)$ and $n = 1, \dots, N$. To highlight the appearance of non-vertical transitions, let us compute the biorthogonal eigenbasis of H_{\pm} under OBC, which are identical upon left/right interchange. We have

$$\langle x | u_{\pm,n}^R \rangle = e^{\pm h(N+1)/2} \sqrt{\frac{2}{N+1}} \sin(k_n x) e^{\mp h x}. \quad (10)$$

Physically, the non-vanishing value of h indicates that the modes in the two non-Bloch bands are squeezed toward the two opposite ends of the lattice (skin effect). The effective dipole moment between OBC eigenstates $|u_{+,n}^R\rangle$ and $|u_{-,l}^R\rangle$ reads

$$\mu_{n,l}^{(\text{eff})} = d_y \sinh(2h) \frac{(e^{h(1+N)} - (-e^{-h})^{(1+N)})(\cos \theta_- - \cos \theta_+)}{2(1+N)(\cosh 2h - \cos \theta_-)(\cosh 2h - \cos \theta_+)} \quad (11)$$

with $\theta_{\pm} = k_n \pm k_l$. Note that $\mu_{n,l}^{(\text{eff})}$ is non-vanishing even for non-vertical transitions $n \neq l$. This means that, under appropriate resonance forcing, ROs can be induced between non-vertical modes, as shown in Fig. 3. Note that, in the large N limit, $\Omega_R \sim e^{hN}/|n-l|^2$, which scales exponentially with hN and to the inverse square of $|n-l|$. The exponential scaling with system size, arising from the skin effect, provides the enhancement of the Rabi frequency, while the inverse power-law dependence on $|n-l|$ indicates that non-vertical transitions, with decreasing strengths as $|n-l|$ increases, are allowed when $h \neq 0$. Examples of enhanced ROs in a lattice comprising $N = 31$ sites for increasing values of the non-Hermitian parameter κ_1/κ_2 are shown in Fig. 4.

More generally, we expect to observe ROs as long as the imaginary parts of the eigenenergies of $H_{\pm} = H_O \pm H_C$ are identical, even if they are not related by imaginary flux

deformations $Q_{\pm}H_H(k - ih_{\pm})$ as assumed above. In particular, the GBZs of H_{\pm} are not fundamentally constrained to be circular. For instance, consider a class of models where $H_C(k) = h_C \mathbb{I}$, $h_C(k)$ a real constant, and H_O possessing a generic GBZ such that $H_O(k + ip(k))$ gives its OBC spectrum. In this case, the spectra of H_{\pm} are related by real energy offsets $\pm h_C$ under both PBCs and OBCs, and thus support ROs. Indeed, ROs allows access into the dynamical properties of such Hamiltonians with non-circular GBZs, which more often than not possess spectra with "arms" extending into the complex energy plane⁴⁴.

Stability of quasi-energies and anharmonic ROs. Non-vertical transitions and boundary-induced dipole enhancement can invalidate the crude RWA, with the appearance of a complex quasi-energy spectrum (Fig. 5), indicating that the system enters into an unstable regime and ROs are not anymore observed, as shown in the "Methods". For the periodically driven lattice, one should calculate the complex quasi-energies using Floquet theory and associated two-dimensional lattices in space-frequency plane, as illustrated in Fig. 6a–c. The onset of complex quasi-energies can be regarded as a kind of parametric instability of the ac-driven system^{65,66}, as indicated by the appearance of unstable resonance tongues in the frequency–amplitude plane, (ω, F_0) , emanating from some of the transition frequencies ω_{nl} (see Figs. 7 and 8). The instability can be physically explained from the field-induced coupling between the two chains H_+ and H_- that makes it possible a secular amplification of excitation along closed loops (Fig. 6c). We remark that breakdown of the RWA and the onset of unstable dynamics is a genuine boundary-driven non-Hermitian effect arising from non-vertical transitions, i.e., it is not related to counter-rotating terms like in the ultrastrong coupling regime of light–matter interaction. An example of the stability domain in the (F_0, h) plane, for fixed value of lattice site N and modulation frequency ω far from any resonance tongue, is shown in Fig. 5a. To observe oscillatory (Rabi-like) dynamics, parameter should be chosen in the stable domain. The largest enhancement factor of effective dipole moment in RO is thus ultimately limited by the onset of the instability, as shown in Fig. 5b. Interestingly, as the system parameters are varied inside the stability domain to approach the stability boundary, ROs become highly anharmonic (see Fig. 4), a phenomenon which is clearly impossible to be observed in any Hermitian lattice.

Discussion

The fundamental processes of absorption and emission of quanta in crystals, as well as coherent Rabi flopping, are deeply modified by edge effects when considering non-Hermitian lattices displaying the skin effect. In particular, boundary-driven non-vertical transitions and anharmonic coherent Rabi flopping can be observed. Such results challenge the common wisdom that bulk coherent processes in crystals are largely independent of boundaries, indicating that skin effects not only question the bulk-boundary correspondence but also coherent bulk phenomena. Owing to the recent experimental progresses in the realization of synthetic non-Hermitian lattices displaying the non-Hermitian skin effect in photonic⁶⁷, mechanical⁶⁸, and electrical circuit^{42,69} platforms, as well as pertinent theoretical advances in cold atom engineering⁷⁰, we expect that the disclosed distinctive physics of absorption and emission of energy in non-Hermitian crystals could be experimentally accessible in the near future.

Methods

GBZ for systems with open boundary conditions. In the absence of the non-Hermitian skin effect, the OBC and PBC eigenstates can be mapped one another in a simple way, and it is physically expected that PBC transitions remain mostly unchanged upon the introduction of open boundaries in a large system. Indeed, for

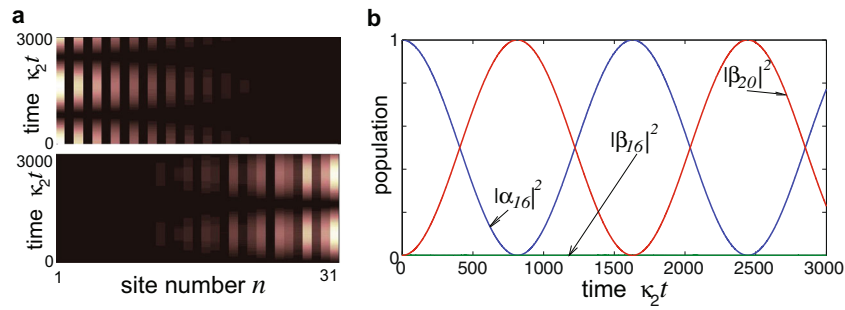


Fig. 3 Rabi oscillations involving non-vertical transitions. The figure shows Rabi oscillations in a non-Hermitian lattice comprising $N = 31$ unit cells with open boundary conditions for parameter values $\Delta/\kappa_2 = 3$, $F_0/\kappa_2 = 0.005$ and $\kappa_1/\kappa_2 = 0.1$. The initial state is the bulk eigenstate $|\mathbf{u}_{+,n}^R\rangle$ with quasi-momentum $k_n = n\pi/(N+1)$ and $n = (N+1)/2 = 16$. The modulation frequency ω is tuned to put in resonance the modes k_n and k_l (with $l = n + 4 = 20$) in the upper and lower bands. **a** Evolution of the real-space occupation probabilities $|A_n|^2$ and $|B_n|^2$ (upper and lower panels). Different k modes are visible from different fringes in upper and lower panels. **b** Evolution of the occupation probabilities $|\alpha_{16}|^2$ and $|\beta_{16}|^2$. Also the probability $|\beta_{20}|^2$ is shown, which remains almost zero because of chosen ac modulation frequency.

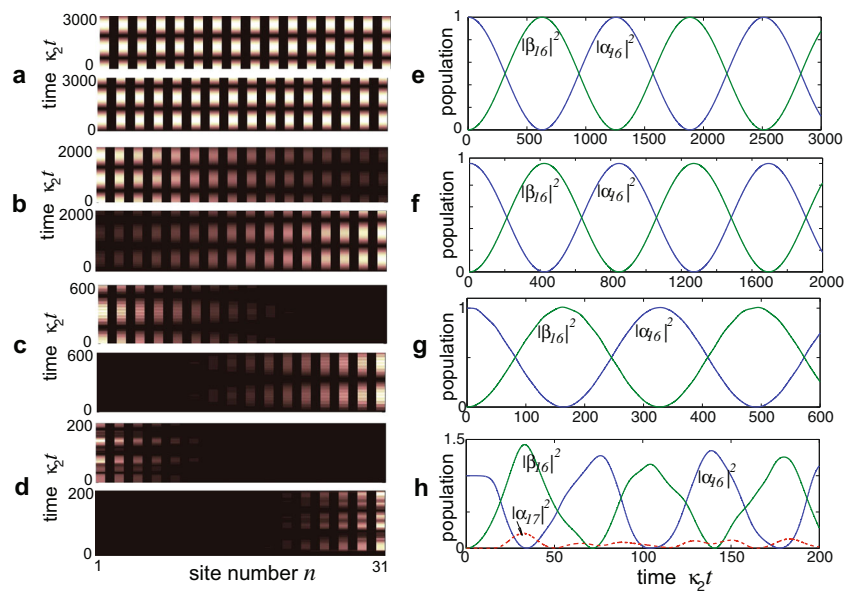


Fig. 4 Ultrafast and anharmonic Rabi oscillations. The figure illustrates enhanced Rabi oscillation frequency induced by skin effect and anharmonic Rabi oscillations for increasing non-Hermitian parameter, measured by the ratio κ_1/κ_2 of amplitude probabilities. Temporal evolution of the real-space occupation probabilities $|A_n|^2$ and $|B_n|^2$ on a pseudocolor map for **a** $\kappa_1/\kappa_2 = 0$ (Hermitian limit), **b** $\kappa_1/\kappa_2 = 0.05$, **c** $\kappa_1/\kappa_2 = 0.1$, and **d** $\kappa_1/\kappa_2 = 0.16$. Other parameter values are $N = 31$ lattice unit cell, $\Delta/\kappa_2 = 3$, $\omega = 2\Delta$, and $F_0/\kappa_2 = 0.005$. The initial state is the bulk eigenstate $|\mathbf{u}_{+,n}^R\rangle$ with quasi-momentum $k_n = n\pi/(N+1)$ and $n = (N+1)/2 = 16$. Temporal evolution of the occupation probabilities $|\alpha_{16}|^2$ (blue curves) and $|\beta_{16}|^2$ (green curves) for **e** $\kappa_1/\kappa_2 = 0$ (Hermitian limit), **f** $\kappa_1/\kappa_2 = 0.05$, **g** $\kappa_1/\kappa_2 = 0.1$, and **h** $\kappa_1/\kappa_2 = 0.16$. In **h** the evolution of $|\alpha_{17}|^2$ is also depicted (dashed red curve), indicating the emergence of mixed and anharmonic Rabi oscillations.

Hermitian lattices with NN hopping and vanishing asymmetry ($h = 0$), the OBC eigenstates [Eq. (10)] are simply odd superpositions of PBC eigenstates with Bloch profiles $e^{\pm ik_n x}$, where $k_n = \frac{n\pi}{N+1}$, $n = 1, \dots, N$ to give rise to N unique OBC states (defined slightly differently from the PBC k_n). The introduction of the non-Hermitian skin effect ($h \neq 0$) amounts just to an exponential factor that can be obtained by deforming the quasi-momentum via $k_n \rightarrow k_n \pm ih$. In this simple example, it is clear that n is still a well-defined label of the eigenstates, even though they are no longer in Bloch form.

More generally, there exists an almost 1-to-1 correspondence between the OBC and PBC eigenstates through the introduction of a GBZ. Intuitively, most of the eigenvalues of the PBC spectrum will adiabatically “flow” en masse towards the OBC eigenvalues when the system is continuously interpolated between PBCs and OBCs, i.e., by slowly switching off the end-to-end couplings, as detailed in ref. 28. In other words, most of the PBC eigenstates, which will have evolved into OBC bulk eigenstates in the absence of the skin effect, will evolve together as boundary-localized skin eigenstates under the skin effect. The exceptions, if any, are topological eigenstates that evolve separately from the rest^{28,31}.

Recently, an “unraveling” picture for the GBZ was developed⁴⁴ to explain how the most general set of skin eigenstates $\mathbf{u}_n^{\text{OBC}}$ for the system with hopping asymmetry h can be understood in terms of non-analytic complex momentum

deformations of PBC eigenstates. This complex momentum lives in the so-called GBZ. First, we introduce the concept of the surrogate Hamiltonian \tilde{H} which does not experience the skin effect, defined via a complex momentum deformation of the physical Hamiltonian H in momentum space:

$$\tilde{H}^{\text{PBC}}(k) = H^{\text{PBC}}(k - i\rho(k)). \quad (12)$$

Here $\rho(k)$ is the complex momentum deformation required such that there exist a double degeneracy in the decay lengths of the eigenstates, i.e., $\rho(k)$ is determined by the condition that for each k , there exists another k' such that the energy dispersion obeys $E(k + i\rho(k)) = E(k' + i\rho(k'))$ with $\rho(k) = \rho(k')$ ^{28,44}. In Hermitian cases, we always have $\rho(k) = 0$ because as k varies over a period, the energy dispersion $E(k)$ must always retrace itself before going back to its original value after a period in k .

To intuitively understand why the $\rho(k) = \rho(k')$ gives rise to a surrogate Hamiltonian that does not experience the skin effect, consider explicitly constructing wave functions that satisfy OBC from superpositions of the PBC momentum eigenstates. If the superposition coefficients were to converge in the thermodynamic limit, we need the presence of bulk-boundary correspondence, i.e., the absence of the skin effect. At a particular energy E , OBC wave functions must satisfy two boundary conditions, namely that they vanish at both ends, i.e., at $x = 0$ and at $x = N + 1$. A superposition of at least two nonzero eigenstates is required for

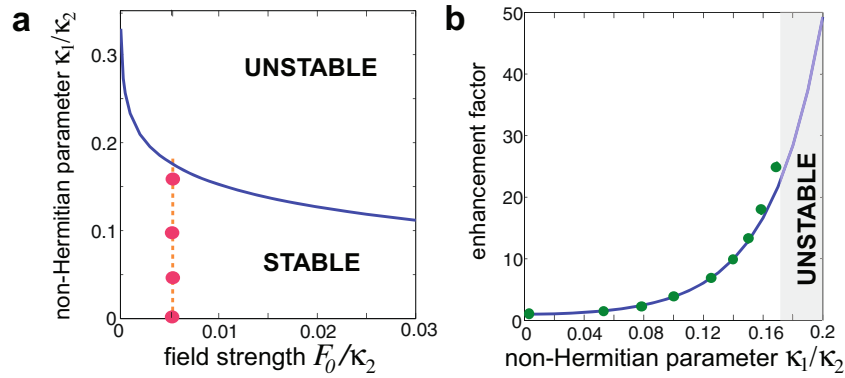


Fig. 5 Stability domain of Rabi flopping. **a** Stability domain of quasi-energies in the plane of normalized forcing amplitude F_0/κ_2 and non-Hermitian parameter κ_1/κ_2 . Parameter values are $\Delta/\kappa_2 = 3$, $\omega = 2\Delta$, and $N = 31$. In the unstable domain quasi-energies are complex, corresponding to exponentially diverging amplitudes. The circles in the stable region correspond to a normalized forcing amplitude $F_0/\kappa_2 = 0.005$. **b** Behavior of the effective dipole $\mu_{n,n}^{(eff)}/d_y$ versus the non-Hermitian parameter κ_1/κ_2 for the same parameter values as in **a** and for the bulk mode corresponding to $k_n = \pi/2$, i.e., $n = (N + 1)/2 = 16$. The solid curve shows the theoretical prediction, while the circles are obtained from the full numerical simulations.

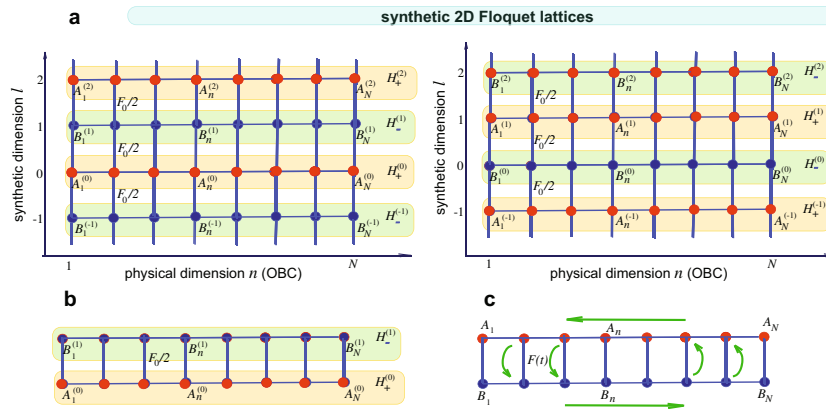


Fig. 6 Floquet lattices. **a** Equivalent decoupled two-dimensional Floquet lattices of the ac-driven system. Different shading denote alternating Floquet chains $H_+^{(l)}$ and $H_-^{(l)}$ in the lattice coupled by the forcing amplitude $F_0/2$, where $l = 0, \pm 1, \pm 2, \dots$ is the Floquet (synthetic dimension) order. **b** Reduced model under wide gap and near-resonant forcing. **c** Simple physical explanation of the onset of instability. In the absence of forcing, excitations are squeezed toward the two opposite edges of the upper and lower chain, and amplification is prevented by the open boundary conditions. As the ac field is switched on, chain coupling realizes closed loops (schematically depicted by arrows), along which excitation can be secularly amplified, resulting in a complex quasi-energy spectrum.

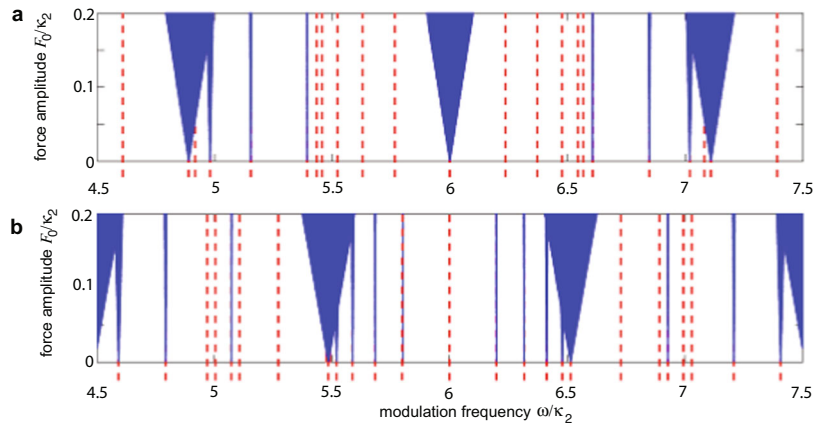


Fig. 7 Stability domain and resonance tongues. Resonance tongues (shaded areas), showing the onset of complex quasi-energies, in the forcing-frequency plane (F_0, ω) for number N of lattice sites **a** $N = 10$, and **b** $N = 11$. Other parameter values are $\kappa_1/\kappa_2 = 0.1$ and $\Delta/\kappa_2 = 3$. The forcing F_0 and frequency ω are normalized to the hopping amplitude κ_2 . The dashed vertical lines in the plots show the position of the various resonance transition frequencies $\omega_{n,l} \equiv (E_{+,n} - E_{-,l})$ between the open boundary condition energy levels in upper and lower bands. Note that the unstable resonance tongues emerge from some (but not all) the resonance transitions.

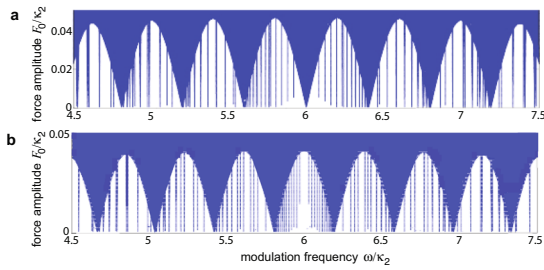


Fig. 8 Stability domain and resonance tongues. Resonance tongues (shaded areas) showing the onset of complex quasi-energies in the forcing-frequency plane (F_0, ω) for number N of lattice sites **a** $N = 30$ and **b** $N = 31$. Other parameter values are $\kappa_1/\kappa_2 = 0.1$ and $\Delta/\kappa_2 = 3$. The forcing F_0 and frequency ω are normalized to the hopping amplitude κ_2 . The dashed vertical lines in the plots show the position of the various resonance transitions at frequencies $\omega_{n,l} \equiv (E_{+,n} - E_{-,l})$ between the open boundary condition energy levels in upper and lower bands.

the wavefunction to vanish at $x = 0$. For it to also vanish at $x = N + 1$ in the thermodynamic limit of arbitrarily large N , another prerequisite is that both eigenstates must decay at the same rate, for otherwise one of them will be infinitesimally small compared to the other, and cannot possibly cancel it off at $x = N + 1$. This requirement that both eigenstates decay at the same rate is just that their imaginary momentum components are equal, i.e., $\rho(k_n) = \rho(k_m)$. This is thus also the condition for \bar{H} to experience no skin effect.

Under OBC where momentum ceases to be a good quantum number, the complex momentum deformation $k \rightarrow k - i\rho(k)$ can be expressed as a similarity transform S with a complex gauge field, i.e.,

$$\bar{H}^{\text{OBC}} = S^{-1}H^{\text{OBC}}S. \quad (13)$$

An important corollary of this is that PBC Hamiltonians related by Eq. (12) possess identical OBC spectra. Hence, to understand the OBC spectrum of a generic non-Hermitian Hamiltonian H , it suffices to determine that of its surrogate Hamiltonian \bar{H} , which is also almost equal to the PBC spectrum of \bar{H} since the latter obeys the bulk-boundary correspondence. In the thermodynamic limit where almost all states (except for isolated edge states) are skin states, the OBC spectrum E^{OBC} is thus almost exactly indexed by $E^{\text{PBC}}(k_n - i\rho(k_n))$.

From Eq. (13), $u^{\text{OBC}} = S\bar{u}^{\text{OBC}}$, both with the same eigenenergy. Since \bar{u}^{OBC} is not a skin state, it can be expanded in terms of the PBC eigenstates, i.e., $\bar{u}_n^{\text{OBC}} = \sum_{n'} c_{nn'} \bar{u}_n^{\text{PBC}}(k_{n'})$ where n, n' label the eigenstates (the label is given through k_n in the PBC case) and $c_{nn'}$ are coefficients that converge in the thermodynamic limit. Hence

$$\begin{aligned} u_n^{\text{OBC}} &= S \bar{u}_n^{\text{OBC}} \\ &= S \sum_{n'} c_{nn'} \bar{u}_n^{\text{PBC}}(k_{n'}) \\ &= \sum_{n'} c_{nn'} \bar{u}_n^{\text{PBC}}(k_{n'} + i\rho(k_{n'})). \end{aligned} \quad (14)$$

For our case of one-band Hamiltonians H_{\pm} , $k_n = \frac{n\pi}{N+1}$, $\bar{u}_n^{\text{PBC}}(k_{n'}) \propto e^{ik_{n'}x}$ and $\rho(k_{n'}) = h \operatorname{sgn}(\sin k_{n'})$. Together, these yield Eq. (10), with biorthogonal normalization imposed.

Vertical transitions in systems with OBCs. In the main text, we discussed vertical and non-vertical transitions between the effective chains governed by Hamiltonians H_{\pm} . Under PBCs, their eigenstates $u_{\pm,n}$ are labeled by the integer n through the quantized lattice quasi-momentum $k_n = 2\pi n/N$, and it is clear that vertical transitions refer to those connecting $u_{+,n}$ and $u_{-,n}$ of the same n and thus quasi-momentum. Under OBCs, however, no well-defined lattice momentum exists, and one should discuss how the notions of vertical/non-vertical transitions can be extended more generally.

The Ansatz $H_{\pm}(k) = Q_{\pm}H_H(k - ih_{\pm})$ used in the main text produces H_{\pm} with real and identical OBC spectra. Since the ih_{\pm} complex deformation can be implemented as a similarity transform $S = \operatorname{diag}(1, e^{ih_{\pm}}, e^{2ih_{\pm}}, \dots, e^{(N-1)ih_{\pm}})$ in real space under OBCs, it is evident that $H_{\pm}(k)$ must possess identical OBC spectra up to a sign Q_{\pm} [see also Eq. (13)].

More generally, constant complex momentum deformations $k \rightarrow k + ik_0$ (k_0 a constant) generate an equivalence class of models with identical OBC spectra. In particular, since $H_H(k + i0)$ is Hermitian, the OBC spectrum must be real. This construction holds for multiband models as well, where we can further generalize the definition of H_{\pm} to $H_{\pm}(k) = Q_{\pm}U^{-1}H_H(k - ih_{\pm})U$ where U is a unitary transformation.

The eigenstates of H_{\pm}^{OBC} can be inferred from Eq. (14) with $\rho(k) = -h_{\pm}$, where \bar{H} is just H_H . Importantly, it is clear how the n th eigenstates of H_{\pm} correspond with

each other. Again, specializing to our one-band model, we shall recover the expression of Eq. (10).

Having established the correspondence between the spectra and eigenstates of H_{\pm} , the notion of vertical ($n = m$) versus non-vertical ($n \neq m$) transitions is well-defined.

Quasi-energy spectrum and stability of ROs. The quasi-energy spectrum of the ac-driven lattice under OBC can be determined by a standard Floquet analysis of Eq. (2), or likewise of Eqs. (5) and (6). Let us assume a sinusoidal driving field $F(t) = F_0 \cos(\omega t)$, and let us search for a solution to Eq. (2) in the form of a Floquet eigenstate, i.e.

$$\mathbf{A}(t) = \sum_l \mathbf{A}^{(l)} \exp(-i\mu t + i\omega l t), \quad \mathbf{B}(t) = \sum_l \mathbf{B}^{(l)} \exp(-i\mu t + i\omega l t), \quad (15)$$

where μ is the quasi-energy, which is uniquely defined in the range $(-\omega/2, \omega/2)$. Substitution of the Ansatz (15) into Eq. (2) given in the main text yields the Floquet chains

$$\mu \mathbf{A}^{(l)} = H_+^{(l)} \mathbf{A}^{(l)} + \frac{F_0}{2} (\mathbf{B}^{(l+1)} + \mathbf{B}^{(l-1)}), \quad \mu \mathbf{B}^{(l)} = H_-^{(l)} \mathbf{B}^{(l)} + \frac{F_0}{2} (\mathbf{A}^{(l+1)} + \mathbf{A}^{(l-1)}), \quad (16)$$

where we have set $H_{\pm}^{(l)} \equiv H_{\pm} + l\omega$. The quasi-energies μ can be thus viewed as the eigenenergies of two decoupled static 2D lattices (stripes), in which one dimension (labeled by the index l , varying from $-\infty$ to ∞) is a synthetic (frequency) dimension while the other dimension (labeled by the index n , varying from $n = 1$ to $n = N$) is the physical space, as schematically shown in Fig. 6a. A special case is the one in which the two non-Bloch bands, defined by the Hamiltonians H_+ and H_- under OBC, are entirely real and spaced by a wide gap 2Δ , like in the model of Fig. 1. Under near-resonant driving $\omega \simeq 2\Delta$ and assuming weak forcing, application of standard multiple-scale asymptotic analysis (see, e.g., ref. 71) indicates that the full Floquet chains of Fig. 6a basically decouple into equivalent quasi 1D static lattices, as shown in Fig. 6b. Thus, at leading order the $2N$ quasi-energies μ of the ac-driven system are obtained as the eigenvalues of the linear system

$$\mu \mathbf{A}^{(0)} = H_+ \mathbf{A}^{(0)} + \frac{F_0}{2} \mathbf{B}^{(1)}, \quad \mu \mathbf{B}^{(1)} = (H_- + \omega) \mathbf{B}^{(1)} + \frac{F_0}{2} \mathbf{A}^{(0)}. \quad (17)$$

Let us specialize the general theory to the model discussed in the main text [Fig. 1 and Eq. (8)]. For given values of the band spacing 2Δ and non-Hermitian deformation parameter h , the quasi-energy spectrum μ turns out to be strongly sensitive to the modulation frequency ω , force strength F_0 , and site number N (in particular N odd or even). Extended numerical simulations, based either on diagonalization of the full Floquet chains (Fig. 6a) or the reduced quasi 1D lattice (Fig. 6b), indicate the existence of multi-branch instability domains in (ω, F_0) space made of wide and narrow resonance tongues, where the quasi-energy spectrum becomes complex. In such regions the amplitudes exponentially grow in time and the observation of oscillatory (Rabi-like) dynamics is thus prevented. Figures 7 and 8 show typical behaviors of resonance tongues for N odd and N even. Interestingly, the unstable resonance tongues emerge from some (but not all) of the transition frequencies $\omega_{n,l} \equiv (E_{+,n} - E_{-,l})$ between OBC energy levels in upper and lower bands. Physically, the onset of the instability can be readily explained from the diagram of Fig. 6c. Forward (backward) propagating excitations in the upper chain are attenuated (amplified) by the imaginary gauge field h . The opposite holds for the lower chain. In the undriven case ($F = 0$), the two chains are decoupled. Owing to the OBC, under steady state the excitations in each chain are squeezed at opposite edges and cannot grow/decay anymore: this means that the energy spectrum remains entirely real despite the non-Hermitian term κ_1 in the Hamiltonian. When the ac force is switched on, closed loops between upper and lower chains, with an overall net amplification of excitation per round trip, are allowed by the vertical solid bonds in Fig. 6c, resulting in complex quasi-energies. In other words, the ac force effectively changes boundary conditions allowing periodic circulation of excitations between the two chains.

Data availability

All relevant data are available from the authors upon request.

Received: 13 March 2020; Accepted: 4 August 2020;

Published online: 26 August 2020

References

- Callaway, J. *Quantum Theory of the Solid State* (Academic Press, New York, 1974).
- Dunlap, D. H. & Kenkre, V. M. Dynamic localization of a charged particle moving under the influence of an electric field. *Phys. Rev. B* **34**, 3625–3633 (1986).

3. Holthaus, M. Collapse of minibands in far-infrared irradiated superlattices. *Phys. Rev. Lett.* **69**, 351–354 (1992).
4. Zhao, X.-G., Georgakis, G. A. & Niu, Q. Rabi oscillations between Bloch bands. *Phys. Rev. B* **54**, R5235–R5238 (1996).
5. Madison, K. W., Fischer, M. C., Diener, R. B., Niu, Q. & Raizen, M. G. Dynamical Bloch band suppression in an optical Lattice. *Phys. Rev. Lett.* **81**, 5093–5096 (1998).
6. Grifoni, M. & Hänggi, P. Driven quantum tunneling. *Phys. Rep.* **304**, 229–354 (1998).
7. Fischer, M. C., Madison, K. W., Niu, Q. & Raizen, M. G. Observation of Rabi oscillations between Bloch bands in an optical potential. *Phys. Rev. A* **58**, R2648–R2651 (1998).
8. Diez, E., Gomez-Alcala, R., Domínguez-Adame, F., Sanchez, A. & Berman, G. P. Rabi oscillations in semiconductor superlattices. *Phys. Rev. B* **58**, 1146–1149 (1998).
9. Platero, G. & Aguado, R. Photon-assisted transport in semiconductor nanostructures. *Phys. Rep.* **395**, 1–157 (2004).
10. Longhi, S. et al. Observation of dynamic localization in periodically-curved waveguide arrays. *Phys. Rev. Lett.* **96**, 243901 (2006).
11. Garanovich, I. L., Longhi, S., Sukhorukov, A. A. & Kivshar, Y. V. Light propagation and localization in modulated photonic lattices and waveguides. *Phys. Rep.* **518**, 1–17 (2012).
12. Lignier, H. et al. Dynamical control of matter-wave tunneling in periodic potentials. *Phys. Rev. Lett.* **99**, 220403 (2007).
13. Makris, K. G., Christodoulides, D. N., Peleg, O., Segev, M. & Kip, D. Optical transitions and Rabi oscillations in waveguide arrays. *Opt. Express* **16**, 10309–10314 (2008).
14. Shandarova, K. et al. Experimental observation of Rabi oscillations in photonic lattices. *Phys. Rev. Lett.* **102**, 123905 (2009).
15. Haller, E. et al. Inducing transport in a dissipation-free lattice with super Bloch oscillations. *Phys. Rev. Lett.* **104**, 200403 (2010).
16. Kudo, K. & Monteiro, T. S. Theoretical analysis of super-Bloch oscillations. *Phys. Rev. A* **83**, 053627 (2011).
17. Alfassi, B., Peleg, O., Moiseyev, N. & Segev, M. Diverging Rabi oscillations in subwavelength photonic lattices. *Phys. Rev. Lett.* **106**, 073901 (2011).
18. Eckardt, A. Atomic quantum gases in periodically driven optical lattices. *Rev. Mod. Phys.* **89**, 011004 (2017).
19. Fistul, M. V. & Efetov, K. B. Electromagnetic-field-induced suppression of transport through n-p junctions in graphene. *Phys. Rev. Lett.* **98**, 256803 (2007).
20. Kibis, O. V. Metal-insulator transition in graphene induced by circularly polarized photons. *Phys. Rev. B* **81**, 165433 (2010).
21. Zhou, Y. & Wu, M. W. Optical response of graphene under intense terahertz fields. *Phys. Rev. B* **83**, 245436 (2011).
22. Crespi, A., Corrielli, G., Della Valle, G., Osellame, R. & Longhi, S. Dynamic band collapse in photonic graphene. *N. J. Phys.* **15**, 013012 (2013).
23. Rudner, M. S. & Song, J. C. W. Self-induced Berry flux and spontaneous non-equilibrium magnetism. *Nat. Phys.* **15**, 1017–1021 (2019).
24. Xiong, Y. Why does bulk boundary correspondence fail in some non-Hermitian topological models. *J. Phys. Commun.* **2**, 035043 (2018).
25. Yao, S. & Wang, Z. Edge states and topological invariants of non-Hermitian systems. *Phys. Rev. Lett.* **121**, 086803 (2018).
26. Kunst, F. K., Edvardsson, E., Budich, J. C. & Bergholtz, E. J. Biorthogonal bulk-boundary correspondence in non-hermitian systems. *Phys. Rev. Lett.* **121**, 026808 (2018).
27. Yao, S., Song, F. & Wang, Z. Non-Hermitian Chern bands. *Phys. Rev. Lett.* **121**, 136802 (2018).
28. Lee, C. H. & Thomale, R. Anatomy of skin modes and topology in non-Hermitian systems. *Phys. Rev. B* **99**, 201103(R) (2019).
29. Martínez Álvarez, V. M., Barrios Vargas, J. E. & Foa Torres, L. E. F. Non-Hermitian robust edge states in one dimension: anomalous localization and eigenspace condensation at exceptional points. *Phys. Rev. B* **97**, 121401(R) (2018).
30. Lee, C. H. et al. Tidal surface states as fingerprints of non-Hermitian nodal knot metals. Preprint at <https://arxiv.org/abs/1812.02011> (2018).
31. Lee, C. H., Li, L. & Gong, J. Hybrid higher-order skin-topological modes in nonreciprocal systems. *Phys. Rev. Lett.* **123**, 016805 (2019).
32. Longhi, S. Loschmidt echo and fidelity decay near an exceptional point. *Ann. Phys.* **531**, 190005 (2019).
33. Ghatak, A. & Das, T. New topological invariants in non-Hermitian systems. *Matter* **31**, 263001 (2019).
34. Yokomizo, K. & Murakami, S. Non-Bloch band theory for non-Hermitian systems. *Phys. Rev. Lett.* **123**, 066404 (2019).
35. Longhi, S. Probing non-Hermitian skin effect and non-Bloch phase transitions. *Phys. Rev. Res.* **1**, 023013 (2019).
36. Song, F., Yao, S. & Wang, Z. Non-Hermitian topological invariants in real space. *Phys. Rev. Lett.* **123**, 246801 (2019).
37. Longhi, S. Topological phase transition in non-Hermitian quasicrystals. *Phys. Rev. Lett.* **122**, 237601 (2019).
38. Edvardsson, E., Kunst, F. K. & Bergholtz, E. J. Non-Hermitian extensions of higher-order topological phases and their biorthogonal bulk-boundary correspondence. *Phys. Rev. B* **99**, 081302(R) (2019).
39. Wang, H., Ruan, J. & Zhang, H. Non-Hermitian nodal-line semimetals with an anomalous bulk-boundary correspondence. *Phys. Rev. B* **99**, 075130 (2019).
40. Imura, K.-I. & Takane, Y. Generalized bulk-edge correspondence for non-Hermitian topological systems. *Phys. Rev. B* **100**, 165430 (2019).
41. Kawabata, K., Shiozaki, K., Ueda, M. & Sato, M. Symmetry and topology in non-Hermitian physics. *Phys. Rev. X* **9**, 041015 (2019).
42. Helbig, T. et al. Generalized bulk-boundary correspondence in non-Hermitian topoelectrical circuits. *Nat. Phys.* **16**, 747–750 (2020).
43. Li, L., Lee, C. H. & Gong, J. Geometric characterization of non-Hermitian topological systems through the singularity ring in pseudospin vector space. *Phys. Rev. B* **100**, 075403 (2019).
44. Lee, C. H., Li, L., Thomale, R. & Gong, J. Unraveling non-Hermitian pumping: emergent spectral singularities and anomalous responses. Preprint at <https://arxiv.org/abs/1912.06974> (2019).
45. Yoshida, T., Mizoguchi, T. & Hatsugai, Y. Mirror skin effect and its electrical circuit simulation. *Phys. Rev. Res.* **2**, 022062(R) (2020).
46. Yang, Z., Zhang, K., Fang, C. & Hu, J. Auxiliary generalized Brillouin zone method in non Hermitian band theory. Preprint at <https://arxiv.org/abs/1912.05499> (2019).
47. Yi, Y. & Yang, Z. Non-Hermitian skin modes induced by on-site dissipations and chiral tunneling effect. Preprint at <https://arxiv.org/abs/2003.02219> (2020).
48. Zhang, X.-X. & Franz, M. Non-Hermitian exceptional Landau quantization in electric circuits. *Phys. Rev. Lett.* **124**, 046401 (2020).
49. Borgnia, D. S., Kruchkov, A. J. & Slager, R.-J. Non-Hermitian boundary modes and topology. *Phys. Rev. Lett.* **124**, 056802 (2020).
50. Zhang, X. & Gong, J. Non-Hermitian Floquet topological phases: exceptional points, coalescent edge modes, and the skin effect. *Phys. Rev. B* **101**, 045415 (2020).
51. Longhi, S. Non-Bloch-band collapse and vohral Zener tunneling. *Phys. Rev. Lett.* **124**, 066602 (2020).
52. Okuma, N., Kawabata, K., Shiozaki, K. & Sato, M. Topological origin of non-Hermitian skin effects. *Phys. Rev. Lett.* **124**, 086801 (2020).
53. Mu, S., Lee, C. H., Li, L. & Gong, J. Emergent Fermi surface in a many-body non-Hermitian fermionic chain. Preprint at <https://arxiv.org/abs/1911.00023> (2019).
54. Bergholtz, E. J., Budich, J. C. & Kunst, F. K. Exceptional topology in non-Hermitian systems. Preprint at <https://arxiv.org/abs/1912.10048v2> (2020).
55. Zhou, L. & Gong, J. Non-Hermitian Floquet topological phases with arbitrarily many real-quasienergy edge states. *Phys. Rev. B* **98**, 205417 (2018).
56. Zhou, L. Dynamical characterization of non-Hermitian Floquet topological phases in one dimension. *Phys. Rev. B* **100**, 184314 (2019).
57. Lee, C. H. & Song, J. C. W. Quenched topological boundary modes can persist in a trivial system. <https://arxiv.org/abs/2002.11726> (2020).
58. Alase, A., Cobanera, E., Ortiz, G. & Viola, L. Exact solution of quadratic fermionic Hamiltonians for arbitrary boundary conditions. *Phys. Rev. Lett.* **117**, 076804 (2016).
59. Alase, A., Cobanera, E., Ortiz, G. & Viola, L. Generalization of Bloch's theorem for arbitrary boundary conditions: Theory. *Phys. Rev. B* **96**, 195133 (2017).
60. Cobanera, E., Alase, A., Ortiz, G. & Viola, L. Generalization of Bloch theorem for arbitrary boundary conditions: Interfaces and topological surface band structure. *Phys. Rev. B* **98**, 245423 (2018).
61. Kunst, F. K., AnMiert, G. V. & Bergholtz, E. J. Extended Bloch theorem for topological lattice models with open boundaries. *Phys. Rev. B* **99**, 085427 (2019).
62. Hatano, N. & Nelson, D. R. Localization transitions in non-Hermitian quantum mechanics. *Phys. Rev. Lett.* **77**, 570–573 (1996).
63. Gong, Z. et al. Topological phases of non-Hermitian systems. *Phys. Rev. X* **8**, 031079 (2018).
64. Lee, J. Y., Ahn, J., Zhou, H. & Vishwanath, A. Topological correspondence between Hermitian and non-Hermitian systems: anomalous dynamics. *Phys. Rev. Lett.* **123**, 206404 (2019).
65. D'Ambroise, J., Malomed, B. A. & Kevrekidis, P. G. Quasi-energies, parametric resonances, and stability limits in ac-driven PT-symmetric systems. *Chaos* **24**, 023136 (2014).
66. Longhi, S. Tight-binding lattices with an oscillating imaginary gauge field. *Phys. Rev. A* **94**, 022102 (2016).
67. Xiao, L. et al. Observation of non-Hermitian bulk-boundary correspondence in quantum dynamics. *Nat. Phys.* **16**, 761–766 (2020).

68. Ghatak, A., Brandenbourger, M., van Wezel, J. & Coulais, C. Observation of non-Hermitian topology and its bulk-edge correspondence. Preprint at <https://arxiv.org/abs/1907.11619> (2019).
69. Hofmann, T. et al. Reciprocal skin effect and its realization in a topoelectrical circuit. *Phys. Rev. Res.* **2**, 023265 (2020).
70. Li, L., Lee, C. H. & Gong, J. Topology-induced spontaneous non-reciprocal pumping in cold-atom systems with loss. *Phys. Rev. Lett.* **124**, 250402 (2020).
71. Longhi, S. Coherent control of tunneling in driven tight-binding chains: perturbative analysis. *Phys. Rev. B* **77**, 195326 (2008).

Acknowledgements

C.H.L. acknowledges research funding by Singapore Ministry of Education Academic Research Fund Tier I (WBS No. R-144-000-435-133). S.L. acknowledges the Spanish State Research Agency through the Severo Ochoa and María de Maeztu Program for Centers and Units of Excellence in R&D (MDM-2017-0711).

Author contributions

S.L. conceived the idea of Rabi flopping in non-Hermitian systems and performed the numerical simulations. S.L. and C.H.L. developed the theory. All authors have discussed and interpreted the results and have written and edited the manuscript.

Competing Interests

The authors declare no competing interests.

Additional information

Supplementary information is available for this paper at <https://doi.org/10.1038/s42005-020-00417-y>.

Correspondence and requests for materials should be addressed to C.H.L. or S.L.

Reprints and permission information is available at <http://www.nature.com/reprints>

Publisher's note Springer Nature remains neutral with regard to jurisdictional claims in published maps and institutional affiliations.



Open Access This article is licensed under a Creative Commons Attribution 4.0 International License, which permits use, sharing, adaptation, distribution and reproduction in any medium or format, as long as you give appropriate credit to the original author(s) and the source, provide a link to the Creative Commons license, and indicate if changes were made. The images or other third party material in this article are included in the article's Creative Commons license, unless indicated otherwise in a credit line to the material. If material is not included in the article's Creative Commons license and your intended use is not permitted by statutory regulation or exceeds the permitted use, you will need to obtain permission directly from the copyright holder. To view a copy of this license, visit <http://creativecommons.org/licenses/by/4.0/>.

© The Author(s) 2020